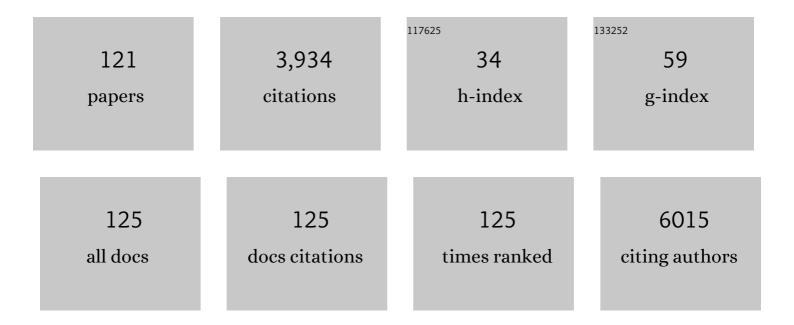
List of Publications by Year in descending order

Source: https://exaly.com/author-pdf/1623236/publications.pdf Version: 2024-02-01



#	Article	IF	CITATIONS
1	Rapid tumoritropic accumulation of systemically injected plateloid particles and their biodistribution. Journal of Controlled Release, 2012, 158, 148-155.	9.9	177
2	InÂVivo Measurement of Age-Related Stiffening in the Crystalline Lens by Brillouin Optical Microscopy. Biophysical Journal, 2011, 101, 1539-1545.	0.5	174
3	Endoscopic Time-Lapse Imaging of Immune Cells in Infarcted Mouse Hearts. Circulation Research, 2013, 112, 891-899.	4.5	161
4	Neutrophils disturb pulmonary microcirculation in sepsis-induced acuteÂlung injury. European Respiratory Journal, 2019, 53, 1800786.	6.7	160
5	In vivo wide-area cellular imaging by side-view endomicroscopy. Nature Methods, 2010, 7, 303-305.	19.0	155
6	Amelioration of sepsis by TIE2 activation–induced vascular protection. Science Translational Medicine, 2016, 8, 335ra55.	12.4	151
7	In vivo tracking of 'color-coded' effector, natural and induced regulatory T cells in the allograft response. Nature Medicine, 2010, 16, 718-722.	30.7	145
8	Lymphatic regulator PROX1 determines Schlemm's canal integrity and identity. Journal of Clinical Investigation, 2014, 124, 3960-3974.	8.2	141
9	Exosome-based delivery of super-repressor lκBα relieves sepsis-associated organ damage and mortality. Science Advances, 2020, 6, eaaz6980.	10.3	132
10	Sustained inflammation after pericyte depletion induces irreversible blood-retina barrier breakdown. JCI Insight, 2017, 2, e90905.	5.0	113
11	In vivo confocal and multiphoton microendoscopy. Journal of Biomedical Optics, 2008, 13, 010501.	2.6	110
12	A Novel Imaging Approach for Early Detection of Prostate Cancer Based on Endogenous Zinc Sensing. Cancer Research, 2010, 70, 6119-6127.	0.9	103
13	Podoplanin-Expressing Cells Derived From Bone Marrow Play a Crucial Role in Postnatal Lymphatic Neovascularization. Circulation, 2010, 122, 1413-1425.	1.6	102
14	Flat amplitude equal spacing 798-channel Rayleigh-assisted Brillouin/Raman multiwavelength comb generation in dispersion compensating fiber. IEEE Photonics Technology Letters, 2001, 13, 1352-1354.	2.5	92
15	Fabrication and operation of GRIN probes for in vivo fluorescence cellular imaging of internal organs in small animals. Nature Protocols, 2012, 7, 1456-1469.	12.0	89
16	Intravital imaging of intestinal lacteals unveils lipid drainage through contractility. Journal of Clinical Investigation, 2015, 125, 4042-4052.	8.2	88
17	Raman-based distributed temperature sensor with simplex coding and link optimization. IEEE Photonics Technology Letters, 2006, 18, 1879-1881.	2.5	84
18	Caspase-8 controls the secretion of inflammatory lysyl-tRNA synthetase in exosomes from cancer cells. Journal of Cell Biology, 2017, 216, 2201-2216.	5.2	81

#	Article	IF	CITATIONS
19	Secreted tryptophanyl-tRNA synthetase as a primary defence system against infection. Nature Microbiology, 2017, 2, 16191.	13.3	76
20	Dynamics of cascaded Brillouin–Rayleigh scattering in a distributed fiber Raman amplifier. Optics Letters, 2002, 27, 155.	3.3	70
21	Optimization of SNR improvement in the noncoherent OTDR based on simplex codes. Journal of Lightwave Technology, 2006, 24, 322-328.	4.6	65
22	A Novel Laser Vaccine Adjuvant Increases the Motility of Antigen Presenting Cells. PLoS ONE, 2010, 5, e13776.	2.5	65
23	Frequency selection rule for high definition and high frame rate Lissajous scanning. Scientific Reports, 2017, 7, 14075.	3.3	59
24	Interaction of tetraspan(in) TM4SF5 with CD44 promotes selfâ€renewal and circulating capacities of hepatocarcinoma cells. Hepatology, 2015, 61, 1978-1997.	7.3	54
25	Polyplex nanomicelle promotes hydrodynamic gene introduction to skeletal muscle. Journal of Controlled Release, 2010, 143, 112-119.	9.9	53
26	In vivo analysis of THz wave irradiation induced acute inflammatory response in skin by laser-scanning confocal microscopy. Optics Express, 2014, 22, 11465.	3.4	51
27	Development of a high speed laser scanning confocal microscope with an acquisition rate up to 200 frames per second. Optics Express, 2013, 21, 23611.	3.4	48
28	Urokinase Exerts Antimetastatic Effects by Dissociating Clusters of Circulating Tumor Cells. Cancer Research, 2015, 75, 4474-4482.	0.9	47
29	Nanoparticle-Assisted Transcutaneous Delivery of a Signal Transducer and Activator of Transcription 3-Inhibiting Peptide Ameliorates Psoriasis-like Skin Inflammation. ACS Nano, 2018, 12, 6904-6916.	14.6	46
30	PM2.5 Exposure in the Respiratory System Induces Distinct Inflammatory Signaling in the Lung and the Liver of Mice. Journal of Immunology Research, 2019, 2019, 1-11.	2.2	43
31	FTY720 Blocks Egress of T Cells in Part by Abrogation of Their Adhesion on the Lymph Node Sinus. Journal of Immunology, 2011, 187, 2244-2251.	0.8	41
32	Establishment of a controlled insulin delivery system using a glucose-responsive double-layered nanogel. RSC Advances, 2015, 5, 14482-14491.	3.6	40
33	In vivo quantitation of injected circulating tumor cells from great saphenous vein based on video-rate confocal microscopy. Biomedical Optics Express, 2015, 6, 2158.	2.9	39
34	Tie2 activation promotes choriocapillary regeneration for alleviating neovascular age-related macular degeneration. Science Advances, 2019, 5, eaau6732.	10.3	39
35	Imaging Laser-Induced Choroidal Neovascularization in the Rodent Retina Using Optical Coherence Tomography Angiography. , 2016, 57, OCT331.		38
36	Lissajous Scanning Two-photon Endomicroscope for In vivo Tissue Imaging. Scientific Reports, 2019, 9, 3560.	3.3	35

#	Article	IF	CITATIONS
37	Dll4 Suppresses Transcytosis for Arterial Blood-Retinal Barrier Homeostasis. Circulation Research, 2020, 126, 767-783.	4.5	35
38	Holographic intravital microscopy for 2-D and 3-D imaging intact circulating blood cells in microcapillaries of live mice. Scientific Reports, 2016, 6, 33084.	3.3	32
39	SNR enhancement of OTDR using biorthogonal codes and generalized inverses. IEEE Photonics Technology Letters, 2005, 17, 163-165.	2.5	28
40	Optical clearing based cellular-level 3D visualization of intact lymph node cortex. Biomedical Optics Express, 2015, 6, 4154.	2.9	28
41	Intravital imaging of a pulmonary endothelial surface layer in a murine sepsis model. Biomedical Optics Express, 2018, 9, 2383.	2.9	28
42	Cross-axis cascading of spectral dispersion. Optics Letters, 2008, 33, 2979.	3.3	26
43	In vivo high spatiotemporal resolution visualization of circulating T lymphocytes in high endothelial venules of lymph nodes. Journal of Biomedical Optics, 2013, 18, 1.	2.6	26
44	Thermoset Elastomers Derived from Carvomenthide. Biomacromolecules, 2015, 16, 246-256.	5.4	25
45	Quinic Acid onjugated Nanoparticles Enhance Drug Delivery to Solid Tumors via Interactions with Endothelial Selectins. Small, 2018, 14, e1803601.	10.0	25
46	Development and evaluation of an ultrasound-triggered microbubble combined transarterial chemoembolization (TACE) formulation on rabbit VX2 liver cancer model. Theranostics, 2021, 11, 79-92.	10.0	22
47	VEGFR2 but not VEGFR3 governs integrity and remodeling of thyroid angiofollicular unit in normal state and during goitrogenesis. EMBO Molecular Medicine, 2017, 9, 750-769.	6.9	21
48	Analysis on the channel power oscillation in the closed WDM ring network with the channel power equalizer. IEEE Photonics Technology Letters, 2000, 12, 1409-1411.	2.5	20
49	Controllable viscoelastic behavior of vertically aligned carbon nanotube arrays. Carbon, 2013, 65, 305-314.	10.3	20
50	Polypeptide-based polyelectrolyte complexes overcoming the biological barriers of oral insulin delivery. Journal of Industrial and Engineering Chemistry, 2017, 48, 79-87.	5.8	20
51	Closed Integral Form Expansion of Raman Equation for Efficient Gain Optimization Process. IEEE Photonics Technology Letters, 2004, 16, 1649-1651.	2.5	19
52	In vivo cellular-level real-time pharmacokinetic imaging of free-form and liposomal indocyanine green in liver. Biomedical Optics Express, 2017, 8, 4706.	2.9	18
53	Intravital longitudinal wide-area imaging of dynamic bone marrow engraftment and multilineage differentiation through nuclear-cytoplasmic labeling. PLoS ONE, 2017, 12, e0187660.	2.5	17
54	Intravital longitudinal imaging of hepatic lipid droplet accumulation in a murine model for nonalcoholic fatty liver disease. Biomedical Optics Express, 2020, 11, 5132.	2.9	17

#	Article	IF	CITATIONS
55	Gradient index lens based combined two-photon microscopy and optical coherence tomography. Optics Express, 2014, 22, 12962.	3.4	15
56	Intraocular Distribution and Kinetics of Intravitreally Injected Antibodies and Nanoparticles in Rabbit Eyes. Translational Vision Science and Technology, 2020, 9, 20.	2.2	15
57	A Novel Pancreatic Imaging Window for Stabilized Longitudinal <i>In Vivo</i> Observation of Pancreatic Islets in Murine Model. Diabetes and Metabolism Journal, 2020, 44, 193.	4.7	15
58	Identification of cromolyn sodium as an anti-fibrotic agent targeting both hepatocytes and hepatic stellate cells. Pharmacological Research, 2015, 102, 176-183.	7.1	14
59	Highly Angiogenic, Nonthrombogenic Bone Marrow Mononuclear Cell–Derived Spheroids in Intraportal Islet Transplantation. Diabetes, 2018, 67, 473-485.	0.6	14
60	Analysis on the transient response of 1.55-μm/1.4-μm dual-wavelength pumped thulium-doped fiber amplifiers. IEEE Photonics Technology Letters, 2002, 14, 1503-1505.	2.5	13
61	In situ design method for multichannel gain of a distributed Raman amplifier with multiwave OTDR. IEEE Photonics Technology Letters, 2002, 14, 1683-1685.	2.5	13
62	In vivo longitudinal cellular imaging of small intestine by side-view endomicroscopy. Biomedical Optics Express, 2015, 6, 3963.	2.9	13
63	In Vivo Fluorescence Retinal Imaging Following AAV2-Mediated Gene Delivery in the Rat Retina. , 2016, 57, 3390.		13
64	Optical clearing assisted confocal microscopy of ex vivo transgenic mouse skin. Optics and Laser Technology, 2015, 73, 69-76.	4.6	12
65	Handheld endomicroscope using a fiber-optic harmonograph enables real-time and in vivo confocal imaging of living cell morphology and capillary perfusion. Microsystems and Nanoengineering, 2020, 6, 72.	7.0	12
66	Novel in-service supervisory system using OTDR for long-haul WDM transmission link including cascaded in-line EDFAs. IEEE Photonics Technology Letters, 2001, 13, 1136-1138.	2.5	11
67	Effect of resveratrol treatment on graft revascularization after islet transplantation in streptozotocin-induced diabetic mice. Islets, 2018, 10, 25-39.	1.8	11
68	3D cellular visualization of intact mouse tooth using optical clearing without decalcification. International Journal of Oral Science, 2019, 11, 25.	8.6	11
69	Study on the gain excursion and tilt compensation for 1.4- and 1.5-î¼m dual wavelength pumped TDFA. IEEE Photonics Technology Letters, 2002, 14, 786-788.	2.5	9
70	Longitudinal Tracing of Spontaneous Regression and Anti-angiogenic Response of Individual Microadenomas during Colon Tumorigenesis. Theranostics, 2015, 5, 724-732.	10.0	9
71	Intravital two-photon imaging and quantification of hepatic steatosis and fibrosis in a live small animal model. Biomedical Optics Express, 2021, 12, 7918.	2.9	9
72	Integral form expansion of fiber Raman amplifier problem. Optical Fiber Technology, 2005, 11, 111-130.	2.7	8

#	Article	IF	CITATIONS
73	Gain and noise figure spectrum control algorithm for fiber Raman amplifiers. IEEE Photonics Technology Letters, 2006, 18, 1125-1127.	2.5	8
74	Stepwise transmigration of T- and B cells through a perivascular channel in high endothelial venules. Life Science Alliance, 2021, 4, e202101086.	2.8	8
75	In vivo longitudinal visualization of the brain neuroinflammatory response at the cellular level in LysM-GFP mice induced by 3-nitropropionic acid. Biomedical Optics Express, 2020, 11, 4835.	2.9	8
76	Integral equation approach for the analysis of high-power semiconductor optical amplifiers. Optics Express, 2006, 14, 2398.	3.4	7
77	Intravital Two-photon Imaging of Dynamic Alteration of Hepatic Lipid Droplets in Fasted and Refed State. Journal of Lipid and Atherosclerosis, 2021, 10, 313.	3.5	7
78	Longitudinal intravital imaging of cerebral microinfarction reveals a dynamic astrocyte reaction leading to glial scar formation. Glia, 2022, 70, 975-988.	4.9	7
79	Multimodal evaluation of an interphotoreceptor retinoid-binding protein-induced mouse model of experimental autoimmune uveitis. Experimental and Molecular Medicine, 2022, 54, 252-262.	7.7	7
80	Estrogen-Related Receptor γ Maintains Pancreatic Acinar Cell Function and Identity by Regulating Cellular Metabolism. Gastroenterology, 2022, 163, 239-256.	1.3	7
81	Quantitative two-photon microscopy imaging analysis of human skin to evaluate enhanced transdermal delivery by hybrid-type multi-lamellar nanostructure. Biomedical Optics Express, 2018, 9, 3974.	2.9	6
82	Two distinct receptor-binding domains of human glycyl-tRNA synthetase 1 displayed on extracellular vesicles activate M1 polarization and phagocytic bridging of macrophages to cancer cells. Cancer Letters, 2022, 539, 215698.	7.2	6
83	Semianalytic dynamic gain-clamping method for the fiber Raman amplifier. IEEE Photonics Technology Letters, 2005, 17, 768-770.	2.5	5
84	Live Images of Donor Dendritic Cells Trafficking via CX3CR1 Pathway. Frontiers in Immunology, 2016, 7, 412.	4.8	5
85	Intravital Imaging of Circulating Red Blood Cells in the Retinal Vasculature of Growing Mice. Translational Vision Science and Technology, 2021, 10, 31.	2.2	5
86	In vivo longitudinal depth-wise visualization of tumorigenesis by needle-shaped side-view confocal endomicroscopy. Biomedical Optics Express, 2019, 10, 2719.	2.9	5
87	Two-photon microscopy by wavelength-swept pulses delivered through single-mode fiber. Optics Letters, 2010, 35, 181.	3.3	4
88	Adiabatic, closed-form approach to the highly efficient analysis of a fiber Raman amplifier problem. Optics Letters, 2005, 30, 126.	3.3	3
89	Imaging cell biology in transplantation. Transplant International, 2016, 29, 1349-1351.	1.6	3
90	Fully packaged video-rate confocal laser scanning endomicroscope using Lissajous fiber scanner. , 2017, , .		3

6

#	Article	IF	CITATIONS
91	Characterization of junctional structures in the gingival epithelium as barriers against bacterial invasion. Journal of Periodontal Research, 2022, 57, 799-810.	2.7	3
92	Novel in-service supervisory scheme for the amplified WDM link with modified optical time domain reflectometry. Optical Fiber Technology, 2002, 8, 139-145.	2.7	2
93	In vivo imaging of the hyaloid vascular regression and retinal and choroidal vascular development in rat eyes using optical coherence tomography angiography. Scientific Reports, 2020, 10, 12901.	3.3	2
94	Micromirror-Embedded Coverslip Assembly for Bidirectional Microscopic Imaging. Micromachines, 2020, 11, 582.	2.9	2
95	Stabilized Longitudinal In Vivo Cellular-Level Visualization of the Pancreas in a Murine Model with a Pancreatic Intravital Imaging Window. Journal of Visualized Experiments, 2021, , .	0.3	2
96	High-performance discrete amplifier based on a second-order fiber Raman oscillator. IEEE Photonics Technology Letters, 2005, 17, 2298-2300.	2.5	1
97	Longitudinal Intravital Imaging of Tumor-Infiltrating Lymphocyte Motility in Breast Cancer Models. Journal of Breast Cancer, 2021, 24, 463-473.	1.9	1
98	Fully packaged confocal endomicroscopic system using Lissajous fiber scanner for indocyanine green in-vivo imaging. , 2018, , .		1
99	In vivo Quantitation of Circulating Tumor Cells by High-speed Intravital Laser-scanning Confocal Microscopy. , 2016, , .		1
100	Quantitative two-photon microscopy imaging analysis of human skin to evaluate enhanced transdermal delivery by hybrid-type multi-lamellar nanostructure: retraction. Biomedical Optics Express, 2020, 11, 5871.	2.9	1
101	3D Visualization of Dynamic Cellular Reaction of Pulpal CD11c+ Dendritic Cells against Pulpitis in Whole Murine Tooth. International Journal of Molecular Sciences, 2021, 22, 12683.	4.1	1
102	Establishment of the reproducible branch retinal artery occlusion mouse model and intravital longitudinal imaging of the retinal CX3CR1-GFP+ cells after spontaneous arterial recanalization. Frontiers in Medicine, 0, 9, .	2.6	1
103	Designing Raman amplified transmission systems: what's there and how to. , 2005, 6019, 424.		0
104	In Vivo Toxicity of Titanium Dioxide and Gold Nanoparticles. , 2012, , 1083-1090.		0
105	Insect Flight and Micro Air Vehicles (MAVs). , 2012, , 1096-1109.		0
106	Intravital laser-scanning microscopy for biomedical research. , 2015, , .		0
107	In vivo quantitation of circulating tumor cells by video-rate intravital laser-scanning confocal microscopy. , 2015, , .		0
108	In vivo analysis of immune cell motility after THz wave irradiation. , 2015, , .		0

#	Article	IF	CITATIONS
109	In vivo lung imaging in pulmonary disease model. , 2015, , .		0
110	In Vivo Real-time Observation of ICG Pharmacokinetics by NIR Laser-scanning Confocal Microscopy. , 2015, , .		0
111	In Vivo Deep Tissue Visualization by Needle-type Side-view Confocal Endomicroscopy. , 2017, , .		0
112	Mouse tissue imaging using real-time Lissajous confocal endomicroscopic system. , 2017, , .		0
113	1457: CAPILLARY ENTRAPMENT OF MAC-1+ NEUTROPHIL DISTURBS PULMONARY MICROCIRCULATION IN SEPSIS-INDUCED ARDS. Critical Care Medicine, 2018, 46, 712-712.	0.9	0
114	Intravital Laser-scanning Two-photon and Confocal Microscopy for Biomedical Research. Medical Lasers, 2021, 10, 1-6.	0.4	0
115	Application of Numerical Analysis Techniques for the Optimization of Wideband Amplifier Performances. , 2006, , 155-172.		0
116	Side-View Endomicroscopy for High-Resolution In Vivo Imaging of the Gastrointestinal Tract. , 2012, , 333-348.		0
117	Intravital Microscopy for THz-Bio Analysis. , 2012, , 413-435.		0
118	In vivo longitudinal cellular imaging of small intestine by side-view confocal endomicroscopy. , 2015, , \cdot		0
119	Intravital Microscopy Analysis. , 2016, , 1698-1708.		0
120	In vivo observation of multiâ€phase spatiotemporal cellular dynamics of transplanted <scp>HSPCs</scp> during early engraftment. FASEB BioAdvances, 0, , .	2.4	0
121	Intravital longitudinal cellular visualization of oral mucosa in a murine model based on rotatory side-view confocal endomicroscopy. Biomedical Optics Express, 2022, 13, 4160.	2.9	0